Available online at www.sciencedirect.com

ScienceDirect

Energy Procedia 55 (2014) 63 – 70

Energy Procedia

4th International Conference on Silicon Photovoltaics, SiliconPV 2014

Quantitative surface recombination imaging of single side processed silicon wafers obtained by photoluminescence modeling

Andreas Fell[a,]*, Daniel Walter[a], Xinbo Yang[a], Sachin Surve[a], Evan Franklin[a], Klaus Weber[a], Daniel MacDonald[a]

[a]*The Australian National University, Canberra 0200, Australia*

Abstract

Characterizing the surface recombination of a silicon wafer is commonly performed by measuring the effective lifetime of a symmetrically processed sample and using simplified analytical models to derive a characteristic property of the recombination, such as the surface recombination factor J_{0s}. The most widely used method is based on QSSPC measurements which require large, homogeneously processed areas and is valid only for uniform carrier distributions throughout the thickness of the sample. In this work we present an alternative method for deriving the surface recombination properties from photoluminescence (PL) images of single side processed wafers, where the rear side minority carrier density is pinned by a highly-recombining surface. By numerically modelling the photoluminescence signal and calibrating it against an independent and well characterized sample, PL images can be quickly converted into, for example, J_{0s} images. We experimentally validate the method and show its robustness and limits by modelling the uncertainty of sample properties and measurement conditions. The method has the advantage of requiring minimal sample preparation. The use of an imaging technique allows numerous parameters to be characterized on a single sample, as is demonstrated by its application to laser-doped silicon.

Peer-review under responsibility of the scientific committee of the SiliconPV 2014 conference

Keywords: luminescence modeling; silicon solar cell; surface recombination; PL imaging; Quokka

* Corresponding author. Tel.: +61 2 6125 2369; fax: +61 2 6125 8873.
E-mail address: andreas.fell@anu.edu.au

Peer-review under responsibility of the scientific committee of the SiliconPV 2014 conference
doi:10.1016/j.egypro.2014.08.075

1. Introduction

Photo-luminescence (PL) and electro-luminescence (EL) imaging is a widely used technique for spatially resolved quantitative analysis of silicon wafers and solar cells. Commonly, analytical models are used to relate the quantity of interest to the measured luminescence signal. The most prominent application is the imaging of excess carrier density and / or effective lifetime [1, 2]. Several other techniques have been developed for imaging a variety of different quantities like series resistance, dark saturation current density and other relevant solar cell parameters [3-6]. Common to most of these techniques is the use of simplified analytical models, most notably in assuming a uniform excess carrier profile across the depth of the sample. In some cases non-uniform carrier profiles have been analytically modeled and utilized to derive quantities sensitive to the carrier profile [7-9]. More advanced techniques also used multidimensional numerical device modeling [10-14].

As it is not possible or at least impractical to model the absolute measured luminescence signal, these techniques generally require calibration, which is typically performed using simultaneous steady-state photo-conductance (SSPC) measurement [1]. In principle this calibration can be done on an independent, accurately characterized sample, so long as the modelling accounts for differences between the relevant properties of the two samples. The validity of such a calibration approach has been shown in [15], where optical differences are modeled, and in [16], where metalized samples are investigated which prohibit a direct PC calibration.

In this work we utilize the free numerical solar cell simulator Quokka for combined electrical device and luminescence modeling [17, 18]. This numerical approach imposes less restrictions on the sample conditions compared to common analytical models, and can thus be used for arbitrary carrier profiles, including lateral non-uniformity [12, 14]. The calibration is done by relating the measured luminescence signal to the simulated one, rather than directly to the quantity of interest. This results in a generally valid calibration factor and consequently in best accuracy when using a calibration sample with (not largely) different characteristics.

This work presents a method to derive front surface recombination images from PL images of a silicon sample with a large variety of uniformly processed regions. Extending on previous work [19, 20], we use a highly recombining rear surface, which is both low-effort to experimentally realize (bare / metalized) [21] and provides a well-defined boundary condition to facilitate accurate modeling. The high rear-surface recombination rate leads to a strong asymmetry in the carrier profile, which makes the PL signal less sensitive to bulk recombination and reduces the effective diffusion length. The latter is valuable in reducing the lateral extents of electronic smearing in the processed region. This reduces its required size while ensuring a homogenous signal in an inner area which is not influenced by its perimeter properties. Besides carrier smear, light smear both in the wafer and the CCD imaging sensor can be significant, and thus has to be carefully considered and mitigated when processing small areas with the potential for large signal gradients [22]. We achieve this by using planar wafers, short-pass filtering and deconvolution to correct for CCD light smear, resulting in suitable areas down to several square-millimeters. This is one to two orders of magnitude below the areas required for QSSPC measurements thereby reducing the sample preparation and characterization effort.

This method was developed in consideration of laser processing, in particular laser doping for localized contacts of silicon solar cells. Here the lowest expected surface recombination is moderately high (surface recombination factor typically $J_{0s} > 500$ fA/cm^2 for metalized highly doped regions) and thus suitable for this method. A large parameter space can therefore quickly be quantitatively characterized with respect to its recombination parameter, significantly enhancing the speed of development and optimization.

We investigate the robustness of the method by modeling uncertainties of sample conditions, and show an application example to illustrate its usefulness.

2. Experimental

We prepared two sets of samples, one for the purpose of calibration and validation and the other for laser doping experiments. Both sets have equivalent surface properties, such that the derived calibration factor from the first sample set is applicable to the second. Thick wafers are used to produce a strong depth-integrated signal, even at the relatively low injection levels which are achieved with low surface lifetimes. Furthermore, to maximize bulk lifetime we chose high resistivity (> 100 Ωcm) n-type FZ wafers, which received a damage etch and cleaning step

before further processing, resulting in wafer thicknesses of 447 µm and 477 µm for the first and second set, respectively.

The first set of samples were ion implanted with boron atoms and subsequently excimer laser annealed [23] across an area suitable for QSSPC measurements. One sample is symmetrically processed, and a second on one side only, with the other side metalized with vacuum-evaporated Aluminum. This ensures that the surface recombination is sufficiently high for accurate modeling (see Fig. 4 *right*), which would not be the case for bare surfaces on high resistivity wafers [21].

The second set of samples was deposited with a boron-rich dielectric, with subsequent laser processing forming highly doped front surface regions. The laser used in this study was a 532 nm nanosecond source with a Gaussian spatial profile, and a focused spot size of approximately 10 µm diameter. The laser processing varied pulse pitch (1 µm – 5 µm), pulse duration (20 ns / 200 ns) and pulse energy across the thresholds of silicon melt and ablation, as determined via visual inspection. For each parameter, we processed areas of 6x2 mm^2 and / or 4x4 mm^2 with overlapping lines.

PL images were taken on a BT LIS R-1 luminescence imaging system, using a 1020 nm shortpass filter to reduce light smear, and a high photon flux (ca. $2.7e^{18}$ $cm^{-2}s^{-1}$ at a laser wavelength of 808 nm) to produce a well measurable signal level.

3. Modeling

We use Quokka as a convenient way to simultaneously perform numerical device and luminescence modeling. Although Quokka requires contacts of both polarities, the contactless PL conditions are well represented by open circuit simulation of a virtually contacted device. One particular advantage over for example PC1D is that Quokka directly accepts an effective surface recombination parameter (effective surface recombination velocity, S_{eff} or J_{0s}), which is the quantity of interest for the presented method. In addition to the relevant sample properties (thickness, bulk resistivity, bulk and surface recombination and internal reflectivity) we also account for the transmission of the filter-lens setup and the sensor EQE, being important to correctly predict the measured signal for different carrier profiles and their corresponding different luminescence spectra. We calculate and apply the wavelength-dependent internal reflectivity for both interfaces considered in this work, which is silicon – air and silicon – Al.

In Fig. 1, an example 1D solution domain and the corresponding steady-state excess carrier profile is shown. Based on this simulation configuration, we establish a relationship between the area-averaged PL signal and the recombination properties of the front surface of the device by performing a number of simulations across a range of surface recombination values. The independent variable of this sweep can be either characteristic property of the surface recombination, S_{eff} or J_{0s}. The luminescence signal at each pixel of the luminescence image can be then converted into a value of recombination by interpolation of the simulated curve. This curve needs to be derived only once for each specific set of sample conditions and only one-dimensional simulations are required, with the required numerical simulations taking only several seconds to compute.

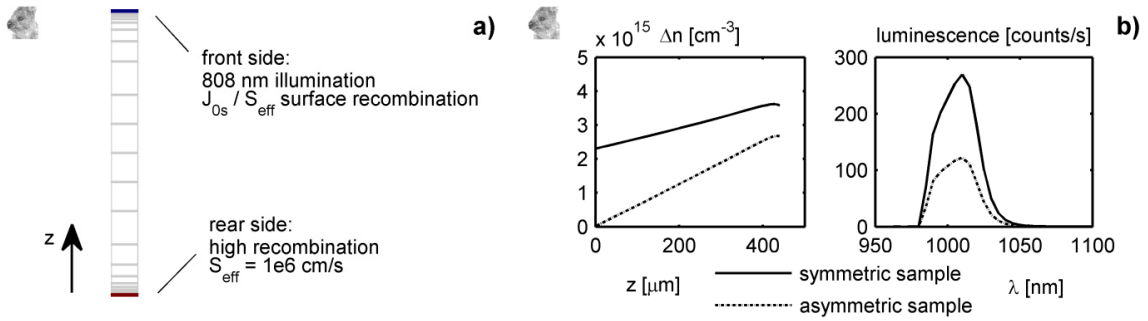

Fig. 1. (**a)** 1D solution domain sketch as used in Quokka; (**b)** example simulated excess carrier profile and luminescence spectrum as detected by the imaging sensor (integration yields the predicted measured PL signal) for the first set of calibration samples and conditions as described in section 2.

4. Results and discussion

4.1. Calibration and validation

The symmetrically ion implanted and excimer laser annealed sample is measured by QSSPC and the value of J_{0s} is then determined by 1D simulations [24] to be 1450 fA/cm^2, assuming an effective intrinsic carrier density at 300K of $n_{ieff} = 9.65e^9$ cm^{-3}. Note that this value for n_{ieff} is consistently used in this work. With this J_{0s}, the PL signal of the symmetric sample under the experimental conditions can be simulated and a calibration factor is derived by relating it to the measured signal. With this calibration, the PL signal of the asymmetric sample, which has an equivalently processed front surface but a highly recombining rear surface is simulated. The simulated signal differs from that measured by less than 2%, as shown in Fig. 2. This level of accuracy is consistent across a range of injection levels (not shown), providing evidence that the calibrated Quokka PL accurately predicts the **measured** PL signal for the strongly asymmetric conditions used in this work.

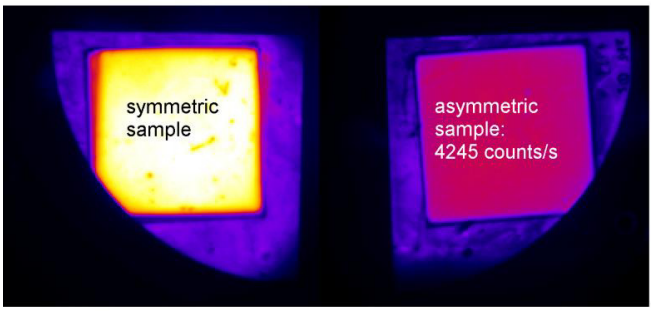

Fig. 2. PL image of the symmetric and asymmetric sample used for calibration and its validation; by using the calibration factor derived from the QSSPC characterized symmetric sample, the PL signal of the asymmetric sample is predicted to 4181 counts/s, which is less than 2% off the measured one.

4.2. Sensitivity analysis

In Fig. 3 the relationship between front surface recombination parameters and PL signal in measurement units is shown. As expected for low front surface recombination the high rear surface recombination dominates, rendering the PL signal essentially insensitive to changes in J_{0s} or S_{eff}. However, for $J_{0s} > 100$ fA/cm^2 or Seff > 100 cm/s, there

is an increasing sensitivity of the PL signal to surface recombination, and thus the method of this work is suitably sensitive above these values.

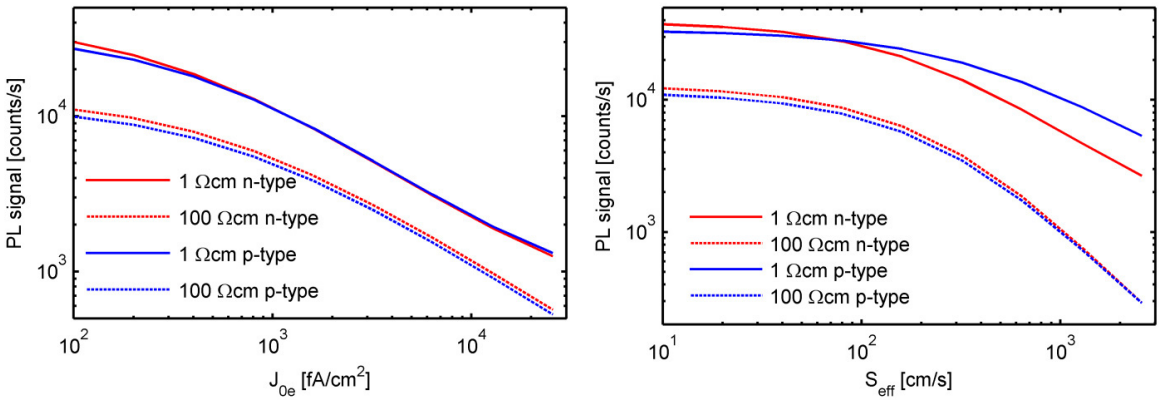

Fig. 3. Relationships between the front surface recombination parameters J_{0s} / S_{eff} and the measured PL signal for 4 different bulk doping levels / types; a suitable sensitivity for this work is given for J_{0s} > 100 fA/cm^2 and S_{eff} > 100 cm/s

Potential error in the plotted relationships arises from uncertainty in the model parameters. Some parameters, such as wafer thickness and bulk resistivity can be determined with suitable accuracy. In addition, uncertainty in laser illumination intensity and the precise optical properties of the sample and imaging system are effectively lumped into the calibration factor and can therefore be considered to not produce a significant error. Another potential error arises by the unknown collection efficiency of the highly doped front region. This means the number of carriers generated and not recombining within the doped region, as this recombination is not accounted for in the modeling by J_{0s}. This source of error was assessed using two extreme cases, defined by 0% and 100% collection efficiency for a 1 µm deep doped region, which revealed no observable difference in the simulated signal. This can be attributed to only a small fraction of the total generation occurring within the highly doped front region for 808 nm illumination, and it can thus be disregarded as a potential source of error.

The main sources of error are identified to be uncertainty in the bulk lifetime, the rear surface recombination parameter, and the accuracy of the calibration factor. Modeling results for a variation of the first two parameters are shown in Fig. 4 for a low resistivity n-type wafer only, however the results are consistent with other values of resistivity and doping types. It is revealed that for a bulk lifetime > 300 µs and a rear surface recombination S_{eff} > 1e^4 cm/s both parameters have no influences on the simulation results. A bulk lifetime above this level can easily be assured by using high-quality FZ material “out-of-the-box”. For moderately to highly doped wafers a bare rear side ensures sufficiently high rear recombination, while for very lowly doped wafers a special treatment or metallization might be required [21]. If those two conditions are ensured, the main remaining error is the inaccuracy of the calibration factor which would linearly scale the predicted PL signal. In this case the error in the QSSPC measurement adds to potential variations between the calibration and test sample which are not accounted for in the modelling. When using very similar samples for calibration the overall error is believed to be dominated by the error of the QSSPC. In conclusion, the calibrated relationship between front surface recombination and PL signal should be accurate to within a couple of percent, although the derived surface recombination parameter will inevitably be less accurate than a direct QSSPC measurement of a suitable sample.

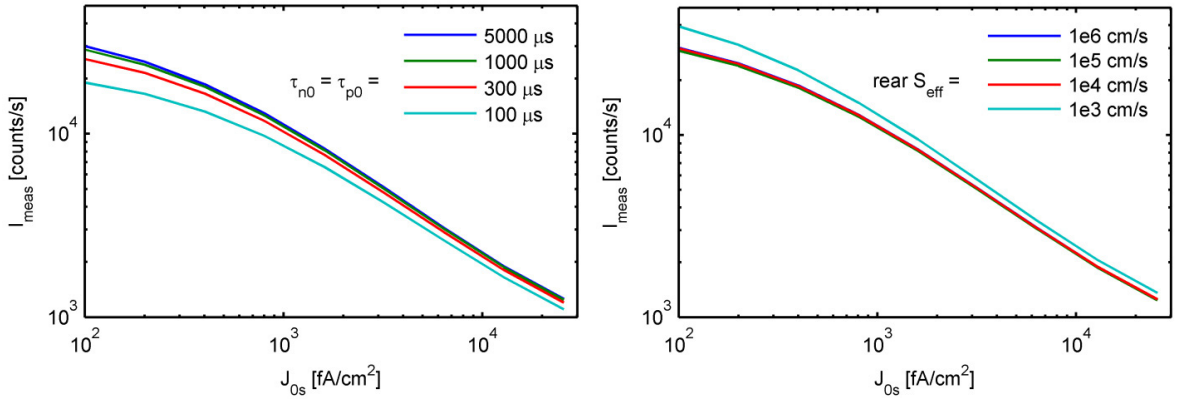

Fig. 4. Sensitivity of the surface recombination – PL relationships to SRH bulk recombination (*left*) and rear surface recombination (*right*) for 1 Ωcm n-type bulk; (not shown) results for other bulk doping levels and types are very similar.

One final source of error potential occurs with the modification of the surface topography by the laser process, as any effective changes to reflectivity and / or the angular distribution of PL emission are not accounted for in the modeling. A well performing laser doping process typically operates below the ablation threshold and results in smooth and optically planar recrystallized surfaces. However, once the ablation threshold of silicon is reached and significant surface roughness is introduced, this error might become significant.

4.3. Laser doping results

Fig. 5 shows the PL image and the corresponding J_{0s} image of the laser doped test sample. The PL image was deconvolved prior to its translation to the J_{0s} image. Apparently the smallest feature size of 6 x 2 mm^2 was not sufficient to isolate the central region from carrier smear, as the signal in the inner region does not approach a constant value across the smaller axis for several laser parameters. However, as some of the small boxes with relatively low J_{0s} values do not show the same effect, this is believed to rather be an actual spatial variation of the J_{0s} values for some of the laser parameters, caused by edge effects during processing. This shows that such a small box size is likely sufficient to quantitatively extract surface recombination parameters, and thus allows for a large parameter variation on a single wafer.

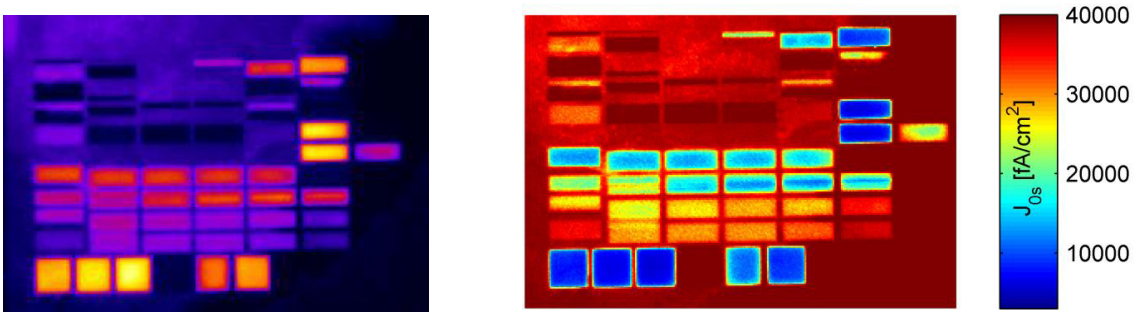

Fig. 5. PL image (*left*) and J_{0s} image (*right*) of a laser doping samples with a large variety of laser parameters derived by pixelwise interpolation to the corresponding curve in Fig. 3; box sizes are 2x6 mm^2 and 4x4 mm^2

5. Conclusions

A method is presented to convert PL images into surface recombination images of a single side processed sample. The rear side is highly recombining, which can be simply ensured by a bare surface or metallization. This lowers the effective lifetime and thus the carrier smear, and also decreases the impact of bulk recombination due to the lower average carrier density in the bulk compared to the front surface. Such a sample is easily prepared and requires only a small, uniformly processed area to ensure that the PL signal is not influence by carrier smear at the process perimeter. By mitigating light smear with planar, specularly reflecting samples, short-pass filtering and deconvolution to correct for CCD sensor light smear, the required minimum area is shown to be in the order of only several square-millimeters.

To model the relationship between surface recombination and PL signal we use Quokka, which conveniently simulates both the carrier transport and luminescence signal. This numerical modeling approach can account for the non-uniform carrier profile and also enables calibration of the simulated PL signal to the measured one using an independent calibration sample. Modeling reveals an unambiguous relationship between the surface recombination parameter of interest (J_{0s} or S_{eff}) and PL signal, if surface recombination is not too low (J_{0s} > 100 fA/cm^2 or Seff > 100 cm/s) and bulk lifetime and rear surface recombination velocity are sufficiently high (SRH bulk lifetime > 300 µs and rear S_{eff} > 1e^4 cm/s).

The method is successfully validated by applying it to samples with symmetric and asymmetric surface recombination properties, the latter having a metalized rear but otherwise identical properties. The predicted and measured PL signal of the asymmetric sample agrees within < 2% across a range of injection levels. It is applied to laser doping experiments using a large variety of laser doping parameters (ca. 50 on a 4 inch wafer quarter). As the number of parameters characterized on a single wafer is orders of magnitude higher than a typical alternative approach using QSSPC for each parameter, this method can vastly reduce the experimental effort for development and optimization of, for example, laser doping processes.

While this work focused on the extraction of a single surface recombination parameter, it can easily be extended to characterize its injection dependence by using multiple illumination levels and simultaneously extracting front excess carrier density.

It is important to note that this method requires uniformly processed areas. This can be a significant limitation in particular for localized laser processing techniques, as processing large areas with overlapping lines might not be representative for the recombination properties of single lines or dots, which are the processes of actual interest. In this case, a extended method can then be applied by processing local features combined with multidimensional modeling [14], however this approach comes at cost of increased feature dimensions and process complexity.

Acknowledgements

The authors acknowledge financial support from the Australian Solar Institute (ASI) / Australian Renewable Energy Agency (ARENA) under the projects 5-F007 and 3-GER002.

References

[1] S. Herlufsen, J. Schmidt, D. Hinken, K. Bothe, and R. Brendel, Photoconductance-calibrated photoluminescence lifetime imaging of crystalline silicon. physica status solidi (RRL) – Rapid Research Letters, vol. 2, pp. 245-247, 2008.

[2] T. Trupke, R. A. Bardos, M. C. Schubert, and W. Warta, Photoluminescence imaging of silicon wafers. Applied Physics Letters, vol. 89, pp. -, 2006.

[3] T. Trupke, E. Pink, R. Bardos, and M. Abbott, Spatially resolved series resistance of silicon solar cells obtained from luminescence imaging. Applied Physics Letters, vol. 90, p. 093506, 2007.

[4] K. Ramspeck, K. Bothe, D. Hinken, B. Fischer, J. Schmidt, and R. Brendel, Recombination current and series resistance imaging of solar cells by combined luminescence and lock-in thermography. Applied Physics Letters, vol. 90, p. 153502, 2007.

[5] M. Kasemann, D. Grote, B. Walter, W. Kwapil, T. Trupke, Y. Augarten, R. Bardos, E. Pink, M. Abbott, and W. Warta, Luminescence imaging for the detection of shunts on silicon solar cells. Progress in Photovoltaics: Research and Applications, vol. 16, pp. 297-305, 2008.

[6] C. Shen, M. A. Green, O. Breitenstein, T. Trupke, M. Zhang, and H. Kampwerth, Improved local efficiency imaging via photoluminescence for silicon solar cells. Solar Energy Materials and Solar Cells, vol. 123, pp. 41-46, 2014.
[7] P. Würfel, T. Trupke, T. Puzzer, E. Schäffer, W. Warta, and S. W. Glunz, Diffusion lengths of silicon solar cells from luminescence images. Journal of Applied Physics, vol. 101, pp. -, 2007.
[8] J. A. Giesecke, M. Kasemann, M. C. Schubert, P. Würfel, and W. Warta, Separation of local bulk and surface recombination in crystalline silicon from luminescence reabsorption. Progress in Photovoltaics: Research and Applications, vol. 18, pp. 10-19, 2010.
[9] B. Michl, J. A. Giesecke, W. Warta, and M. C. Schubert, Separation of Front and Backside Surface Recombination by Photoluminescence Imaging on Both Wafer Sides. Photovoltaics, IEEE Journal of, vol. 2, pp. 348-351, 2012.
[10]S. C. Baker-Finch and K. R. McIntosh, Photoluminescence Imaging Diagnosis of Particulate Iron Contamination Derived From HF Dip and Thermal Oxidation. Photovoltaics, IEEE Journal of, vol. 1, pp. 66-71, 2011.
[11]P. Gundel, F. D. Heinz, M. C. Schubert, J. A. Giesecke, and W. Warta, Quantitative carrier lifetime measurement with micron resolution. Journal of Applied Physics, vol. 108, pp. -, 2010.
[12]M. Juhl, T. Trupke, and Y. Augarten, Emitter sheet resistance from photoluminescence images. in Photovoltaic Specialists Conference (PVSC), 2013 IEEE 39th, 2013, pp. 0198-0202.
[13]M. Padilla, H. Höffler, C. Reichel, H. Chu, J. Greulich, S. Rein, W. Warta, M. Hermle, and M. C. Schubert, Surface recombination parameters of interdigitated-back-contact silicon solar cells obtained by modeling luminescence images. Solar Energy Materials and Solar Cells, vol. 120, Part A, pp. 363-375, 2014.
[14]A. Fell, D. Walter, S. Kluska, E. Franklin, and K. Weber, Determination of Injection Dependent Recombination Properties of Locally Processed Surface Regions. Energy Procedia, vol. 38, pp. 22-31, 2013.
[15]H. C. Sio, S. P. Phang, T. Trupke, and D. Macdonald, An Accurate Method for Calibrating Photoluminescence-based Lifetime Images on Multi-crystalline Silicon Wafers in this conference, 2014.
[16]B. Hallam, Y. Augarten, B. Tjahjono, T. Trupke, and S. Wenham, Photoluminescence imaging for determining the spatially resolved implied open circuit voltage of silicon solar cells. Journal of Applied Physics, vol. 115, pp. -, 2014.
[17]A. Fell, A Free and Fast Three-Dimensional/Two-Dimensional Solar Cell Simulator Featuring Conductive Boundary and Quasi-Neutrality Approximations. Electron Devices, IEEE Transactions on, vol. 60, pp. 733-738, 2013.
[18]A. Fell, K. R. McIntosh, M. Abbott, and D. Walter, Quokka version 2: selective surface doping, luminescence modeling and data fitting. in 23rd Photovoltaic Science and Engineering Conference, Taipei, 2013.
[19]X. Yang, D. Macdonald, A. Fell, A. Shalav, L. Xu, D. Walter, T. Ratcliff, E. Franklin, K. Weber, and R. Elliman, Imaging of the relative saturation current density and sheet resistance of laser doped regions via photoluminescence. Journal of Applied Physics, vol. 114, pp. 053107-053107-6, 2013.
[20]J. Bullock, D. Yan, A. Thomson, and A. Cuevas, Imaging the Recombination Current Pre-factor J0 of Heavily Doped Surface Regions; A Comparison of Low and High Injection Photoluminescence Techniques. in Proceedings of the 27th European Photovoltaic Solar Energy Conference, Frankfurt, Germany, 2012, pp. 1312-1318.
[21]S. Y. Lim, M. Forster, X. Zhang, J. Holtkamp, M. C. Schubert, A. Cuevas, and D. Macdonald, Applications of Photoluminescence Imaging to Dopant and Carrier Concentration Measurements of Silicon Wafers. Photovoltaics, IEEE Journal of, vol. 3, pp. 649-655, 2013.
[22]D. Walter, A. Fell, E. Franklin, D. Macdonald, B. Mitchell, and T. Trupke, The Impact of Silicon CCD Photon Spread on Quantitative Analyses of Luminescence Images. Photovoltaics, IEEE Journal of, vol. 4, pp. 368-373, 2014.
[23]X. Q. e. a. Yang, Boron implanted, laser annealed p+ emitter for n-type interdigitated back-contact solar cells. in this conference, 2014.
[24]A. Thomson, N. Grant, K. F. Chern, and T. Kho, Improved Diffused-Region Recombination-Current Pre-Factor Analysis. in this conference, 2014.